Journal of Magnetic Resonance 205 (2010) 69–74

Contents lists available at ScienceDirect

Journal of Magnetic Resonance

journal homepage: www.elsevier.com/locate/jmr

EPR of Mn^{2+} in the kagomé staircase compound $Mg_{2.97}Mn_{0.03}V_2O_8$

Pavlo Aleshkevych *, Jan Fink-Finowicki, Marek Gutowski, Henryk Szymczak

Institute of Physics PAS, al. Lotnikow 32/46, 02-668 Warsaw, Poland

ARTICLE INFO

Article history:
Received 22 January 2010
Revised 7 April 2010
Available online 10 April 2010

Keywords:
Kagomé structure
EPR

ABSTRACT

The electron paramagnetic resonance (EPR) of Mn^{2+} in geometrically frustrated $Mg_{2.97}Mn_{0.03}V_2O_8$ single crystals is reported. The complex EPR spectrum shows resonance lines associated with two crystallographically nonequivalent lattice positions of Mn ions that are known in the kagomé staircase system as "cross-tie" and "spine" sites. Additionally, strongly anisotropic resonances of various Mn^{2+}–Mn^{2+} pairs are observed. The signs and values of the crystal field parameters are determined from EPR spectra. The local magnetic symmetry details of magnetic ions and components of the hyperfine structure tensor are determined for various nonequivalent manganese positions. The exchange coupling between Mn ions in "cross-tie" and "spine" sites is found to be $J = 41$ K.

1. Introduction

Magnetic materials with geometrical frustration have recently attracted much attention both from the theoretical and experimental side [1]. Of particular interest has been the magnetism of the two-dimensional (2D) kagomé lattices because these systems are highly frustrated due to specific geometry leading to higher order of degeneracy and complexity of magnetic ground states [2,3]. This interest is stimulated by the attempts to find new fundamental effects such as for example the jumps or plateaus of magnetization curves [4,5]. A few examples of the kagome-staircase lattice compounds have been studied widely, mostly $Co_3V_2O_8$ (CVO) [3,6], $Ni_3V_2O_8$ (NVO) [7] and $Mn_3V_2O_8$ (MVO) [8]. It was found that all these systems show rich magnetic field–temperature (H–T) phase diagrams because of buckled kagome lattice breaks ideal triangle symmetry by pushing the competitive magnetically ordered states closer to each other. Also in all the mentioned systems (H–T) diagrams show strong anisotropic behavior depending of magnetic field orientation with respect to the crystallographic axes. It is interesting that a such strong anisotropy is observed not only in CVO having cobalt ions in orbital triplet ground state but also in MVO where Mn^{2+} is in orbital singlet ground state. To get better understanding of kagome buckled systems, it seems to be important to investigate the single-ion anisotropy contribution to the overall anisotropy.

The purpose of this paper is to present the EPR study in $Mg_{2.97}Mn_{0.03}V_2O_8$ single crystals, isostructural with kagome systems MVO, NVO and CVO, focusing on the crystal field effects in doped kagome systems. Earlier, the single-ion anisotropy in CVO was probed by EPR in [9].

The fragment of the generic buckled kagome crystal structure of $Mg_3V_2O_8$ is shown in Fig. 1. There are two crystallographically nonequivalent positions in Mg sublattices that are known in the kagomé staircase system as *spine* and *cross-tie* sites, marked on Fig. 1 as S and C, respectively. The S sites form chains along the a-axis, chains are linked by the C sites in the c direction to form the buckled kagomé staircase, and stacked along the b direction. The S and C sites occupy centers of the oxygen octahedra. The oxygen atoms are labeled with numbers in Fig. 1. The crystallographic data show that oxygen octahedra around *cross-tie* sites are squeezed along c-axis and have axial symmetry (the distances C–O4 and C–O5 are equal to 2.03 nm and 2.13 nm, respectively). The oxygen octahedra around *spine* sites are more distorted (the distances S–O1, S–O2 and S–O3 are equal to 2.11 nm, 2.02 nm and 2.13 nm, respectively) and also slightly tilted from site to site along both a and c axes.

The Mg and V ions are nonmagnetic in pure $Mg_3V_2O_8$ crystal. A small amount of Mg (1%) ions is substituted by isovalent paramagnetic Mn^{2+}. The half-filled d-shell of free Mn^{2+} ion leaves $^6S_{5/2}$ term as a ground state. However in single crystals the Mn^{2+} the ground state is a mixture of an S-term with excited terms in octahedral environment, so the crystal field provides initial zero-field splitting of the ground state levels and, as a rule, the EPR of Mn^{2+} ion shows both fine and hyperfine structure components, due to electron spin $S = 5/2$ and nuclear spin ^{55}Mn $I = 5/2$, respectively [10].

2. Experimental data and analysis

The single crystals of $Mg_{2.97}Mn_{0.03}V_2O_8$ were grown from polycrystalline feed rods by floating zone technique [5]. The

* Corresponding author.
E-mail address: pavloa@ifpan.edu.pl (P. Aleshkevych).

1090-7807/$ - see front matter © 2010 Elsevier Inc. All rights reserved.
doi:10.1016/j.jmr.2010.04.004

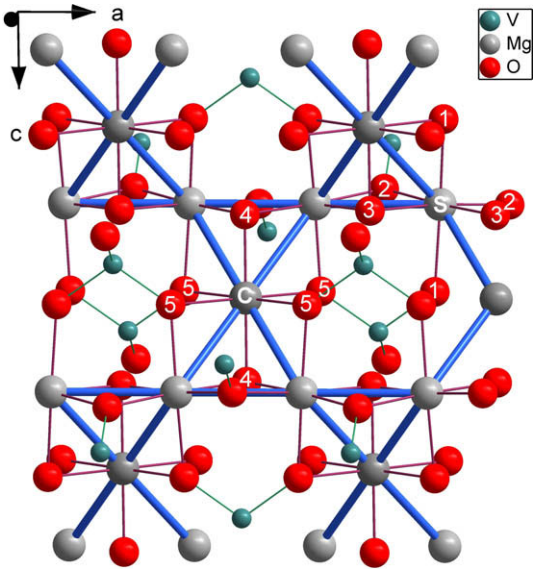

Fig. 1. The fragment of the $Mg_3V_2O_8$ crystal structure in *ac* plane.

investigated single crystals probed by X-ray diffraction technique were found to be single-phase of orthorhombic symmetry (space group *Cmca*) [11] with the lattice parameters very similar to the kagomé staircase compound $Mg_3V_2O_8$ and $Mn_3V_2O_8$. The slab-shaped samples, of about $2 \times 2.3 \times 2.5$ mm^3, were cut from the X-rays oriented single crystal. The EPR measurements were carried out using Bruker EMX spectrometer working at fixed frequency (9.25 GHz) with Oxford Instruments helium-flow cryostat operating in the temperature range from 3.8 K to 300 K. A 100 kHz magnetic field modulation and phase sensitive detection were used to record the derivative of the absorbed microwave power. The samples were glued to a rotatable sample holder to record angular variation of the EPR spectra.

2.1. Single ion spectrum

The EPR spectra were observed at full available temperature range (3.8–300 K). Fig. 2 shows typical EPR spectrum of $Mg_{2.97}Mn_{0.03}V_2O_8$ for the magnetic field parallel to *b*-axis. Two pat-

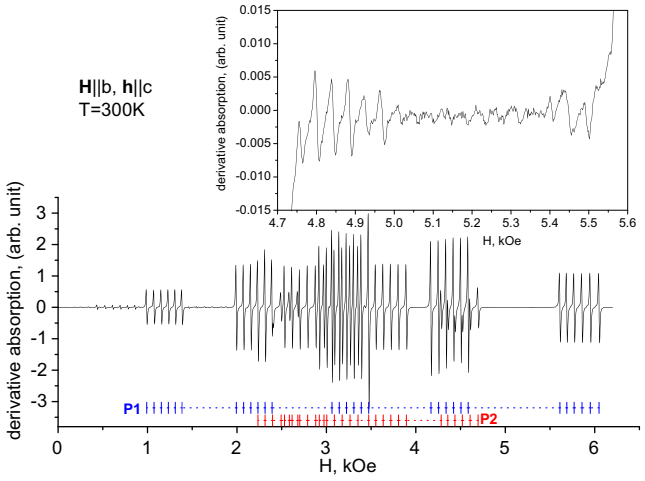

Fig. 2. An example of the EPR spectrum of $Mg_{2.97}Mn_{0.03}V_2O_8$ for $H||b$ recorded at room temperature. The microwave field vector *h* is applied along *c*-axis. Two groups of thirty lines marked as P1 and P2. The inset shows the enlarged fragment of the same spectrum.

terns of 30 lines each characteristic for Mn^{2+} ions located in two nonequivalent positions (labeled as P1 and P2 in Fig. 2) dominate this spectrum. The intensities of resonance lines belonging to P1 are roughly twice larger than those belonging to P2. Since the *spine* sites outnumber twice the *cross-tie* sites, this may suggest that P1 sites correspond to *spine* positions while P2 – to *cross-tie*, if the dopant Mn^{2+} ions are randomly distributed between C and S positions. Besides the main resonance lines, the weak lines attributed to Mn^{2+} pairs were observed as well (shown on inset in Fig. 2). Finally, the low-field ($H < 3$ kOe) part of spectrum exhibits many, more or less intensive, resonance lines originating from "forbidden" transitions which become partially allowed due to strong mixing eigenstates.

The EPR spectra are very anisotropic. To catch out all the details, the angular variations of EPR spectra were measured in three mutually perpendicular planes at room temperature. The angular dependencies of the resonance positions of all visible resonance lines are shown in Fig. 3a–c, for magnetic field *H* rotated in the planes *ab*, *bc*, *ac*, respectively. As it is seen, the angular dependencies for C positions have their extrema coinciding with crystallographic axes while the lines for S positions are split in *ac* plane onto two patterns, symmetrically placed around *c*-axis. The extrema of these patterns are shifted by ±32° away from *c*-axis in the *ac* plane, see Fig. 3c.

The positions of resonance lines of single Mn^{2+} ion are described by the spin-Hamiltonian composed of Zeeman, hyperfine and crystal field terms:

$$\hat{\mathscr{H}} = \mu_B(\vec{H}\tilde{g}\hat{S}) + (\hat{S}\tilde{A}\hat{I}) + \sum_{q\leqslant k} B_k^q Q_k^q(\hat{S}_x, \hat{S}_y, \hat{S}_z) \qquad (1)$$

where μ_B is the Bohr magneton, $\vec{H}$ – the external magnetic field vector, $\hat{S}$ – the spin operator, $\tilde{g}$ and $\tilde{A}$ – the *g*-factor and the hyperfine interactions tensors respectively, $\hat{I}$ – the nuclear spin operator, Q_k^q – Stevens crystal field operators acting on spin and B_k^q – the microscopic crystal field parameters. The Hamiltonian (1) operates in "laboratory" Cartesian coordinates with axes *X*, *Y*, *Z* chosen to coincide with the crystallographic axes *a*, *b*, *c*, respectively.

To describe the experimental data, a special computer program was used throughout this paper to calculate the positions and intensities of the resonance transitions, for both isolated ions and pair Mn spectra. The most time-consuming task was the exact numerical diagonalization of a spin-Hamiltonian, avoiding using perturbation methods. Prior to the diagonalization the complex hermitian matrix of the spin-Hamiltonian was reduced to the real tridiagonal form and next the QL/QR [12] algorithm was applied. For Hamiltonian (1) the basis eigenfunctions were chosen as $|M,m\rangle$, where *M* and *m* are the spin and nuclear magnetic quantum number. The orthorhombic crystal symmetry requires to take into account terms up to the fourth order ($q,k = 0,2,4$) in the crystal field expression (1), however the terms with B_4^2, B_4^4 were found to be small and were neglected. The fitted crystal field parameters B_2^0, B_2^2, B_4^0 for both crystallographic positions are listed in Table 1. The analysis of integral intensity of the resonance transitions belonging to different components of the fine structure as a function of temperature was used to determine the signs of the parameters B_k^q.

The principal values of the $\tilde{g}$ and $\tilde{A}$ tensors for both positions are listed in Table 2

Earlier, the assignment of the groups of resonance lines to two crystallographic positions was made by analyzing their intensities. Now, the analysis of the fitted parameters, together with the crystalographical data, makes possible to have that assignment unambiguous. It follows from Tables 1 and 2 that *cross-tie* sites show nearly axial symmetry $B_2^2 \ll B_2^0$, $g_c < (g_a \approx g_b)$, $A_c < (A_a \approx A_b)$ while the *spine* sites show larger rhombic distortion. This is expected

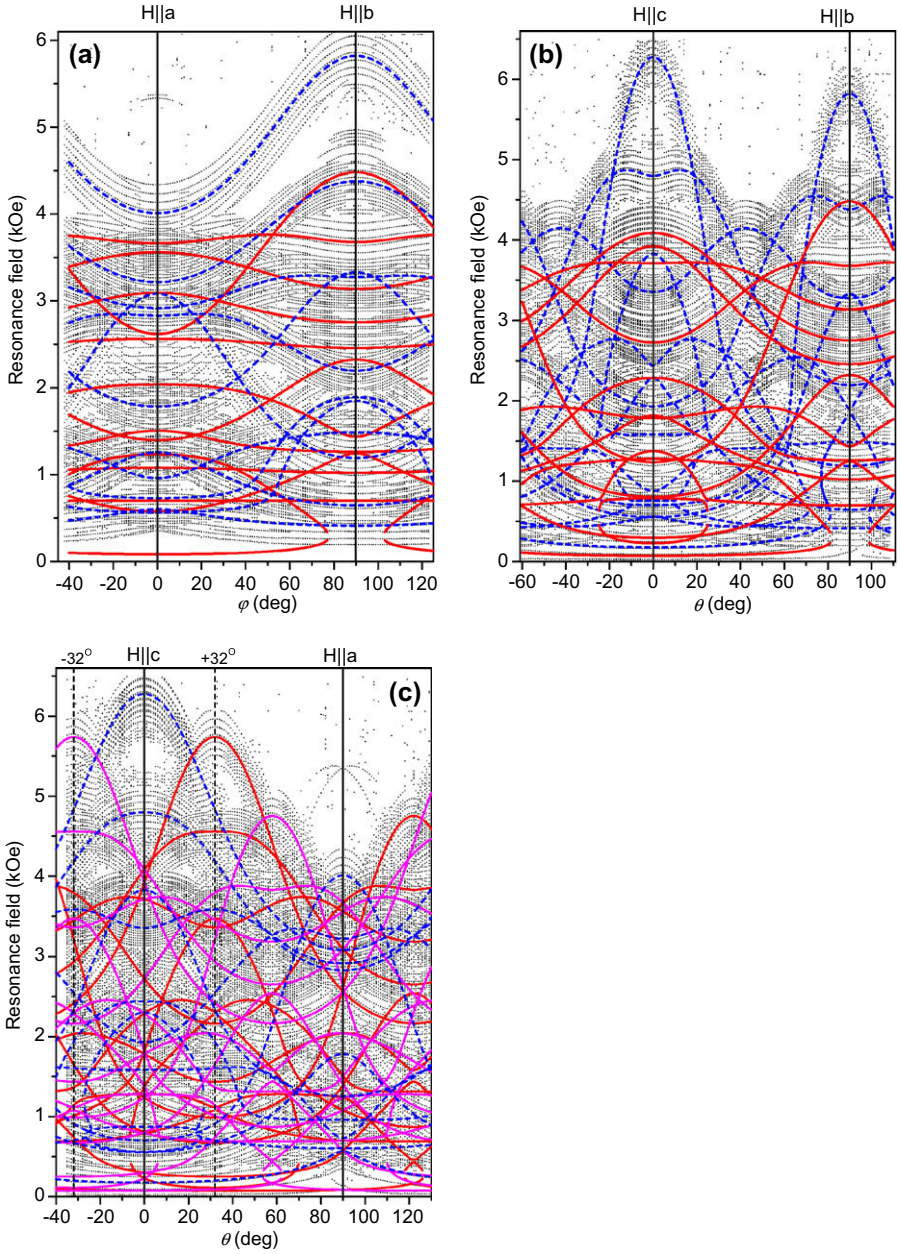

Fig. 3. The angular variation of the resonance fields of all resolved transitions in the EPR spectrum in three mutually perpendicular planes *ab* (a), *bc* (b) and *ac* (c) at $T = 300$ K. φ is the angle between H and a-axis while θ is the angle between H and c-axis. Symbols represent experimental data. The calculated resonance fields shown by dashed and solid lines for P1 and P2 positions, respectively. For clarity of illustration the calculated lines do not account for hyperfine splitting due to the nuclear spin.

Table 1
Crystal field parameters.

Site	B_2^0 cm^{-1}	B_2^2 cm^{-1}	B_4^0 cm^{-1}
P1	227.3×10^{-4}	149.8×10^{-4}	-0.1×10^{-4}
P2	184.8×10^{-4}	-21.9×10^{-4}	0.0×10^{-4}

Table 2
The principal values of the g and A tensors.

Site	g_a	g_b	g_c	A_a ($\times 10^{-4}$ cm^{-1})	A_b ($\times 10^{-4}$ cm^{-1})	A_c ($\times 10^{-4}$ cm^{-1})
P1	2.0022	1.9937	1.9929	76.5 ± 0.5	76.7 ± 0.5	77.5 ± 0.5
P2	1.9989	1.9991	1.9946	82.1 ± 0.5	81.0 ± 0.5	73.1 ± 0.5

from crystallographic data. The local x, y, z-axes of *cross-tie* sites coincide with the laboratory X, Y, Z axes. On the other hand the *spine* sites are divided into two magnetically nonequivalent positions: the local z-axis of *spine* positions are deflected from Z-axis by +32° and −32° in XZ-plane; local y-axis of all *spine* positions coincides with Y-axis.

The simulated positions of the resonance lines, calculated for isolated *spine* and *cross-tie* sites using parameters from Tables 1 and 2 are shown in Fig. 3 by solid and dashed lines. For clarity of illustration these lines were calculated disregarding the hyperfine splitting (HFS) into six lines, due to the nuclear spin.

2.2. Pair spectrum

The concentration of Mn ions in studied crystals is estimated to be about 1%, therefore assuming their random distribution one should expect with roughly 0.01% probability that any given Mn ion will have another Mn ion as its nearest neighbor. Consequently,

one may expect that the Mn–Mn pair spectrum will have two order of magnitude lower intensity than that of isolated Mn^{2+} ion. Such weak resonance lines belonging to the pair spectrum are effectively masked in background by single ions' spectrum, what makes the analysis difficult. Similarly, in the low-field region ($H < 3$ kOe) we can observe the multitude of more or less intensive resonances originating from partially allowed "forbidden" transitions. They become allowed due to strong mixing of energy levels whenever Zeeman splitting is comparable to crystal field effects. Inability to distinguish pair and weak, but numerous, single-ion resonances makes low-field spectrum virtually unusable for our purposes. Therefore the only opportunity to evaluate the information concerning Mn^{2+}–Mn^{2+} interaction strength is to investigate the high-field part of the EPR spectrum. For given values of the crystal field parameters of order $\sim 0.02\ cm^{-1}$, see Table 1, the Zeeman interaction will override other terms in spin-Hamiltonian (1) for magnetic field higher than 3 kOe thus making eigenfunctions of the energy levels looking almost like pure quantum spin states. In this situation the transitions involving of electron magnetic quantum number other than $\Delta M = \pm 1$ are strongly prohibited. So any weak resonance lines in that region are most probably related to the pair spectrum.

An example of resonance lines belonging to pair spectrum was shown in inset in Fig. 2. The positions of resonance lines in the pair spectrum depend strongly on the direction of the magnetic field. A very characteristic peculiarity of the pair spectrum is the hyperfine splitting between lines equal to the half of the value for isolated Mn^{2+} ions. In fact, as it is seen from Fig. 2, the spacing between adjacent lines is close to 42 Oe which is roughly half of average HFS splitting of either *cross-tie* or *spine* sites. Two different kinds of nearest neighbours pairs made of adjacent Mn ions are possible: those located in *cross-tie* and *spine* sites and *spine–spine* ones. The resonance spectrum for both types of pairs is expected to be very complex, because of numeral differences in microscopic parameters characterizing both sites. Even small crystal field acting on Mn ions or any anisotropic exchange interactions will lift degeneracy of the energy levels producing huge number of resonance transitions. In such a case the key role in analysis of pair spectrum is played by precise simulation of EPR spectrum for any given set of microscopic parameters. The same program and algorithm for numerical diagonalization was used for pair spin-Hamiltonian as previously for isolated Mn ion.

The pair spin-Hamiltonian is composed of the sum of two isolated single-ion spin-Hamiltonians and the interaction term

$$\widehat{\mathscr{H}}_{pair} = \sum_{i=1}^{2} \widehat{\mathscr{H}}_i + \widehat{\mathscr{H}}_{1,2} \tag{2}$$

The "laboratory" orthogonal system of coordinates is chosen to coincide with the crystallographic axes *a*, *b*, *c*. The $\widehat{\mathscr{H}}_i$ describes Mn in *cross-tie* or *spine* site as needed with parameters listed in Tables 1 and 2. Since magnetic axes of *spine* site do not coincide with "laboratory" coordinate system, the corresponding matrix of $\widehat{\mathscr{H}}_i$ was rotated around *Y*-axis by + or -32° before diagonalization. The pair interaction term in (2) was chosen in quite common notation as

$$\widehat{\mathscr{H}}_{1,2} = \widehat{S}_1 \widetilde{J} \widehat{S}_2 + J_{biq} (\widehat{S}_1 \widehat{S}_2)^2 \tag{3}$$

where first and second term describe the bilinear and biquadratic exchange interaction, respectively. The $\widetilde{J}$ is a second rank dyadic tensor containing all the relevant exchange parameters.

The eigenfunction basis for Hamiltonian $\widehat{\mathscr{H}}_{pair}$ was chosen as $|M_1, m_1, M_2, m_2\rangle$, where M_i and m_i are the spin and nuclear magnetic quantum number. Upon numerical diagonalization of Hamiltonian (2), the $(2S_1 + 1)(2I_1 + 1)(2S_2 + 1)(2I_2 + 1) = 1296$ (size of matrix) eigenvalues and corresponding eigenfunctions were calculated. The eigenfunctions were found as a linear combination of the basis eigenfunctions.

The numerical simulation of the pair spectrum shows that the most meaningful influence on spectrum comes from diagonal elements of tensor $\widetilde{J}$ which are strictly related to the isotropic part of exchange interaction $J = \frac{1}{3} Tr\{\widetilde{J}\}$ [13]. The exchange constant $|J| > 2\ cm^{-1}$ makes bilinear exchange the dominating term in spin-Hamiltonian (2), especially that crystal field parameters are of order of $0.02\ cm^{-1}$ only. Then that term can be reduced for real spin to the simple form $J\widehat{S}_1\widehat{S}_2$, where the electron spins $S_1 = S_2 = 5/2$ because of $3d^5$ electronic configuration of Mn^{2+} ions. In that case all energy levels of Mn^{2+}–Mn^{2+} pair are grouped into six multiplets starting from singlet, characterized by total spin quantum number $|S_1 - S_2| = 0$ and up to the multiplet with $S_1 + S_2 = 5$. The distance between multiplets is proportional to exchange constant *J* and their ordering is up to the sign of *J*. For antiferromagnetic interaction ($J > 0$), the lowest multiplet is singlet. The degeneracy of each of the multiplets is lifted, even in absence of magnetic field, because of the non-zero crystal field. The small off-diagonal elements of $\widetilde{J}$ related to anisotropic exchange [14], as well as biquadratic exchange interactions, also contribute to the zero-field splitting of multiplets, greatly complicating the pair spectrum.

It is not easy to determine precisely all components of the exchange interaction tensor $\widetilde{J}$, because only the part of resonance lines related to the pair spectrum can be extracted from experimental data. However, the isotropic exchange constant can be found by analyzing the temperature dependence of the integral intensity of resonance lines because the spin multiplets of Mn–Mn pair are thermally activated and the temperature of activation depends on *J*. The intensity of transition I_{mn} between two energy levels E_m and E_n at given temperature *T* can be evaluated by following general formula:

$$I_{mn} = (H_{mn})^2 \frac{N}{\sum_i e^{-\frac{E_i}{kT}}} \left[e^{-\frac{E_m}{kT}} - e^{-\frac{E_n}{kT}} \right] \tag{4}$$

where H_{mn} is the matrix element corresponding to transition I_{mn}; *N* – number of atoms. The summation in denominator runs over all populated levels in the energy spectrum.

The temperature dependence for two resonance lines at $H = 4920$ Oe and $H = 5340$ Oe is shown on Fig. 4. These lines have

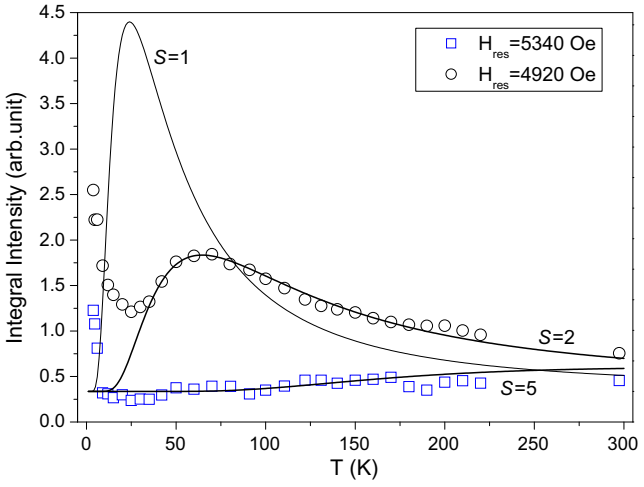

Fig. 4. The temperature dependencies of the integral intensity of the resonance absorptions from Mn^{2+}–Mn^{2+} pair spectrum. The symbols (□) and (○) represent intensity of weak lines (shown in inset in Fig. 2) recorded at $H = 5340$ Oe and $H = 4920$ Oe, respectively. The solid lines show numerically calculated pair spectrum intensities vs. T for transitions within different multiplets: $S = 1, 2, 5$. The calculations use parameters from Tables 1 and 2 and $J = 41$ K.

different temperature dependencies because they correspond to resonance transitions from different multiplets. Numerical simulations of the both *cross-tie–spine* and *spine–spine* pair spectra at $H||b$ and all parameters given from Tables 1 and 2 show that in the 4.7 kOe–5.6 kOe range the resonance transitions from multiplets with total spins $S = 2$ and $S = 5$ are expected, so the resonance line at $H = 4920$ Oe corresponds to multiplet with the total spin $S = 2$ while the line at $H = 5340$ Oe corresponds to the highest lying multiplet with the total spin $S = 5$. Utilizing Eq. (4), the temperature dependences of resonance transitions intensity from different multiplets were calculated and are shown as solid lines on Fig. 4. A good agreement between experimental and calculated dependencies occurs for $J = (41 \pm 2)$ K (28.5 cm^{-1}). It is assumed that within error the J values are the same for both types of pairs.

Such a high values of J separates multiplets one from another so well that effectively eliminates resonance transitions between different multiplets even at high magnetic field. This fact has two good consequences. First, the pair spectrum becomes significantly simplified to only intramultiplets transitions. And second, more important, the resonance fields of transitions in pair spectrum practically do not depend on the value J (except for transitions within multiplet $S = 1$, not resolved in the presented experimental spectra), because isotropic exchange does not affect zero-field splitting. This is in opposition to the non-isotropic exchange interaction, which strongly change the zero-field splitting of multiplets and strongly affects the positions of resonance lines in the pair spectrum. This gives an opportunity to estimate the non-isotropic exchange interactions by studying the angular variation of resonance lines.

The angular variations of the resonance field transitions in the *bc* plane are shown on Fig. 5. The high-field part of the spectrum is shown only, where the pair spectrum transitions are resolved. It follows from the picture that lines show its maxima rathers symmetrically placed with respect to the crystallographic directions *b* and *c*. That means that anisotropic exchange interactions, tending to shift off the extreme positions from main directions, probably can be neglected when compared with the isotropic exchange. However, more precise evaluation of the off-diagonal elements of $\tilde{J}$ tensor requires further investigation. The tensor $\tilde{J}$ can be decomposed into the sum of symmetric and antisymmetric tensors [13]. The antisymmetric tensor is traceless and the symmetric tensor can be made traceless by subtracting diagonal elements describing the isotropic exchange. According to Moriya [15], the elements of such traceless antisymmetric and symmetric tensor are of order $\Delta g/g$ and $(\Delta g/g)^2$ respectively, and they are smaller than the isotropic exchange. In fact, the Mn^{2+} ion has very small anisotropy of the *g*-factor as compared with for example the Co^{2+} or Ni^{2+} ions. One can estimate, based on the values from Table 1, that $\Delta g/g$ is of order of $\sim$0.005 and respectively $(\Delta g/g)^2$ is about $\sim 2 \times 10^{-5}$. Such a small anisotropic exchange cannot influence significantly the EPR spectrum of Mn^{2+}.

Note the presence in Fig. 5 of the group of resonance lines for angles between 40° and 60°, having their local maximum at about 50°. The presence of this group cannot be explained by isotropic or anisotropic exchange only. An appearance of an extremum at intermediate angles is explainable if the biquadratic exchange interaction is present. The numerical simulations, with J_{biq} as a fitting parameter, show that the biquadratic exchange interaction is one order of amplitude bigger for the *spine–spine* pair than that for the *cross-tie–spine* pair. The solid and dashed lines show the angular dependencies of resonance line positions in the pair spectrum best fitted to experimental points for *cross-tie* and *spine–spine* pairs, respectively. The biquadratic exchange constant J_{biq} is found to be 0.04 ± 0.02 K for *spine–spine* pair and 0.0045 ± 0.0025 K for *cross-tie–spine* pair.

Of course, besides nearest neighboring (NN) Mn^{2+}–Mn^{2+} pair, there are other possible configurations: next-nearest neighboring pairs or even clusters consisting of three atoms in triangle, *cross-tie–spine–spine*, but intensity of such configurations is expected to be much smaller than that of NN pairs and was not taken into account.

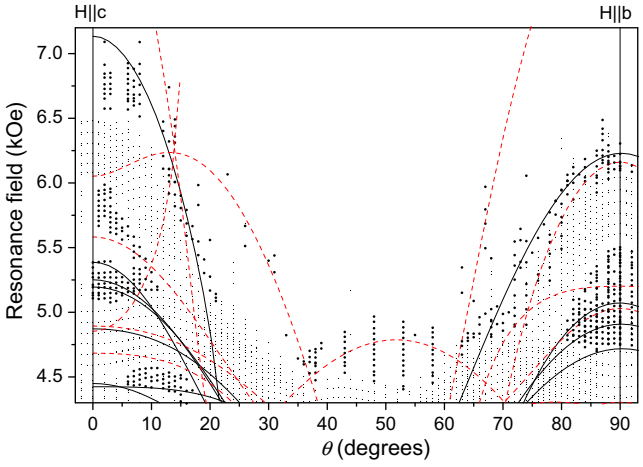

Fig. 5. The angular variation of the resonance field of all observed transitions in EPR spectrum in the *bc* plane at $T = 300$ K. The circles and squares symbols represent experimental data related to the Mn^{2+}–Mn^{2+} pairs and isolated Mn^{2+} ions resonance lines, respectively. The solid and dashed lines show the numerically calculated angular dependencies of resonance line positions best fitted to experimental points of the pair EPR spectrum for *cross-tie–spine* and *spine–spine* pairs, respectively.

3. Conclusions

The local symmetry of oxygen octahedron surrounding Mn ions in *cross-tie* and *spine* positions is found to be different: axial for *cross-tie* and rhombic for *spine*. Moreover, we find unambigously the presence of two magnetically nonequivalent spine type positions of Mn^{2+} ions. The main values of the *g*-factors and hyperfine structure as well as microscopic parameters of the crystal filed are determined for both Mn^{2+} positions. The exchange interaction constant J between NN *cross-tie* and *spine* positions of Mn is found to be 41 K. The anisotropic and biquadratic exchange interactions are also estimated.

Acknowledgments

The work was supported in part by the Ministry of Science and Higher Education Poland through Grant No. N202 057 32/1201.

References

[1] A.P. Ramirez, Geometrical Frustration, vol. 13, Handbook of Magnetic Materials, 2001, p. 423.
[2] B. Canals, C. Lacroix, Phys. Rev. Lett. 80 (1998) 2933.
[3] A.P. Ramirez, A. Hayashi, R.J. Cava, R. Siddhartan, B.S. Shastry, Nature (London) 399 (1999) 333.
[4] K. Kageyama, R. Yoshimura, N. Stern, V. Mushnikov, K. Onizuka, M. Kato, K. Kosuge, C.P. Slichter, T. Goto, Y. Ueda, Phys. Rev. Lett. 82 (1999) 3168.
[5] R. Szymczak, M. Baran, R. Diduszko, J. Fink-Finowicki, M. Gutowska, A. Szewczyk, H. Szymczak, Phys. Rev. B 73 (2006) 1.
[6] Y. Chen, J.W. Lynn, Q. Huang, F.M. Woodward, T. Yildirim, G. Lawes, A.P. Ramirez, N. Rogado, R.J. Cava, A. Aharony, O. Entin-Wohlman, A.B. Harris, Phys. Rev. B 74 (2006) 014430.
[7] G. Lawes, M. Kenzelmann, N. Rogado, K.H. Kim, G.A. Jorge, R.J. Cava, A. Aharony, O. Entin-Wohlman, A.B. Harris, T. Yildirim, Q.Z. Huang, S. Park, C. Broholm, A.P. Ramirez, Phys. Rev. Lett. 93 (2004) 247201.
[8] E. Morosan, J. Fleitman, T. Klimczuk, R.J. Cava, Phys. Rev. B 76 (2007) 144403.
[9] P. Aleshkevych, J. Fink-Finowicki, H. Szymczak, Acta Phys. Pol., A 111 (2007) 105.

[10] A. Abraham, B. Bleaney, Electron Paramagnetic Resonance of Transition Ions, Clarendon Press, Oxford, 1970.
[11] Jason D. Pless, N. Erdman, Donggeun Ko, Laurance D. Marks, Peter C. Stair, Kenneth R. Poeppelmeier, Cryst. Growth Des. 3 (4) (2003) 615.
[12] G.H. Golub, C.F. Van Loan, Matrix Computations, 3rd ed., Johns Hopkins University Press, Baltimore, 1996.
[13] A. Bencini, D. Gatteschi, Electron Paramagnetic Resonance of Exchange Coupled Systems, Springer Verlag, Berlin, 1990.
[14] I. Dzyaloshinsky, Phys. Chem. Solids 4 (1958) 241.
[15] T. Moriya, Phys. Rev. 120 (1960) 91.